SCIENTIFIC REPORTS
nature research

OPEN

Functional interactions between nitrite reductase and nitric oxide reductase from *Paracoccus denitrificans*

Ingrid Albertsson[1], Johannes Sjöholm[1,2], Josy ter Beek[1,3], Nicholas J. Watmough[4], Jerker Widengren[2] & Pia Ädelroth[1*]

Denitrification is a microbial pathway that constitutes an important part of the nitrogen cycle on earth. Denitrifying organisms use nitrate as a terminal electron acceptor and reduce it stepwise to nitrogen gas, a process that produces the toxic nitric oxide (NO) molecule as an intermediate. In this work, we have investigated the possible functional interaction between the enzyme that produces NO; the cd_1 nitrite reductase (cd_1NiR) and the enzyme that reduces NO; the *c*-type nitric oxide reductase (*c*NOR), from the model soil bacterium *P. denitrificans*. Such an interaction was observed previously between purified components from *P. aeruginosa* and could help channeling the NO (directly from the site of formation to the side of reduction), in order to protect the cell from this toxic intermediate. We find that electron donation to *c*NOR is inhibited in the presence of cd_1NiR, presumably because cd_1NiR binds *c*NOR at the same location as the electron donor. We further find that the presence of *c*NOR influences the dimerization of cd_1NiR. Overall, although we find no evidence for a high-affinity, constant interaction between the two enzymes, our data supports transient interactions between cd_1NiR and *c*NOR that influence enzymatic properties of *c*NOR and oligomerization properties of cd_1NiR. We speculate that this could be of particular importance *in vivo* during metabolic switches between aerobic and denitrifying conditions.

Denitrification is an anaerobic process in which nitrate (NO_3^-) is reduced stepwise to nitrogen gas (N_2) via the intermediates nitrite, nitric oxide and nitrous oxide. There is widespread interest in denitrification because it limits the amount of nitrogen available to crops by decreasing the amount of nitrate and nitrite in the soil and because incomplete denitrification yields nitrous oxide which is a potent green-house gas. In *Paracoccus (P.) denitrifi*cans, a model organism for both aerobic respiration and denitrification, the enzymes that catalyze these reactions are: nitrate reductase (NAR), reducing nitrate to nitrite, nitrite reductase (NiR) which reduces nitrite to nitric oxide, nitric oxide reductase (NOR), reducing nitric oxide to nitrous oxide and finally nitrous oxide reductase (N_2OR), which reduces nitrous oxide to nitrogen gas (for a review on denitrification enzymes, see[1]).

The stepwise reduction of nitrate requires the product of one enzyme to be the substrate for the next enzyme in the pathway and as a consequence the expression of all four enzymes should be coordinated and regulated in such way that the concentrations of nitrite and nitric oxide are kept at concentrations that are not toxic to the cell[2]. Lethal nitric oxide concentrations have been shown to vary between organisms, with some bacteria such as *Agrobacterium tumefaciens* accumulating μM NO concentrations during rapid switches between oxic and anoxic conditions, but in *P. denitrificans* nitric oxide is kept at (or below) ~30 nM[3].

The enzyme catalyzing the reduction of nitrite to nitric oxide ($NO_2^- + e^- + 2H^+ \rightarrow NO + H_2O$) in *P. denitrificans* is cytochrome cd_1 nitrite reductase (cd_1NiR), a soluble protein located in the periplasm (for a recent review on cd_1NiR and nitrite, see[4]). The almost identical (97% sequence identity) and well characterized cd_1NiR from *Paracoccus pantotrophus* is purified[5] and crystallized as a dimer[6]. Each cd_1NiR monomer consists of one small

[1]Department of Biochemistry and Biophysics, Stockholm University, Svante Arrhenius väg 16C, SE-106 91, Stockholm, Sweden. [2]Experimental Biomolecular Physics, Department of Applied Physics, Royal Institute of Technology (KTH), SE-106 91, Stockholm, Sweden. [3]Present address: Department of Medical Biochemistry and Biophysics, Umeå University, Umeå, SE-90187, Sweden. [4]School of Biological Sciences, University of East Anglia, Norwich Research Park, Norwich, NR4 7TJ, UK. *email: pia.adelroth@dbb.su.se

heme *c* domain and one large d_1 domain, where NO_2^- reduction takes place. The heme *c* domain receives electrons from one of two soluble donors; either cytochrome c^{550} or the copper protein pseudoazurin[7]. The heme d_1 in the catalytic domain has an unusual ability (as compared to other hemes) to rapidly release NO, thereby lowering the degree to which the cd_1NiR enzyme activity is inhibited by its product NO[8].

The well-characterized cd_1NiRs from *P. pantotrophus* and *Pseudomonas (Ps) aeruginosa* (see e.g.[9] and[4]) have many properties in common including a similar overall fold especially in the larger, catalytic d_1 domain. They also use similar electron donors; a soluble *c* cytochrome or a blue copper protein. However, there are also striking differences, such as the 'domain swapping' that occurs only in the *Ps. aeruginosa* cd_1NiR dimer, where the N-terminal arm (in the cyt. *c* domain) of one monomer crosses over to interact with the d_1 domain of the second monomer.

Nitric oxide, produced from cd_1NiR, is further reduced to nitrous oxide ($2NO + 2e^- + 2H^+ \rightarrow N_2O + H_2O$), by nitric oxide reductase (NOR). NORs are members of the heme-copper oxidase (HCuO) superfamily. This superfamily (comprising the cytochrome *c* oxidase in mitochondria) is large and diverse and some of its members are capable of NO-reduction[10–12], and all that have been investigated also show that the physiological O_2-reduction reaction is inhibited by NO (reviewed in[13,14], see also[15]), an effect which is linked to the use of NO as a signaling molecule in mammals[16].

The NOR from *P. denitrificans* is a cytochrome *c*-dependent NOR (*c*NOR) that, as purified, is composed of two subunits; NorB and NorC. The NorB is an integral membrane protein and harbors a low-spin heme *b* and the active site, composed of a high-spin heme b_3 and a non-heme iron, Fe_B. NorC is membrane-anchored and contains a periplasmic heme *c*, which receives electrons from soluble donors such as cytochrome *c* or pseudoazurin (the same as for cd_1NiR). The enzyme uses protons and electrons from the same side of the membrane (periplasmic, see[17,18]) and is thus non-electrogenic[19,20], which differs from the O_2-reducing HCuOs. The crystal structure of the *c*NOR from *P. aeruginosa* supports this as putative proton transfer pathways are only found leading from the periplasm into the active site[21].

Respiratory chain complexes in mitochondria commonly form higher-order complexes, so-called supercomplexes. Such supercomplexes have also been found in bacteria (see e.g.[22,23]), but the functional advantage of them is not always fully understood. Recently, the crystal structure of a complex between separately purified cd_1NiR and *c*NOR from *Ps. aeruginosa* was presented[24]. The complex has a 2:2 stoichiometry (dimer of cd_1NiR with two monomers of *c*NOR), and the interaction was suggested to be present also under native conditions, but then in a 2:1 stoichiometry since the membrane-location of *c*NOR is not compatible with the 2:2 complex observed. Such a cd_1NiR-*c*NOR complex could confer advantages *in vivo* as the toxic NO molecule would, instead of being released into the periplasmic solution, rather be 'channeled' into the membrane in which it is more soluble. From the membrane, NO could directly enter the gas channel suggested for *c*NOR[21,25], see Fig. 1.

The aim of this work was to determine whether the *P. denitrificans* cd_1NiR and *c*NOR form a molecular complex *in vivo* and/or *in vitro* and to study potential functional interactions *in vitro*. To this end we investigated the localization of cd_1NiR in *P. denitrificans*, and we also used the *c*NOR catalyzed reaction as an *in vitro* 'handle' to report on a possible complex with cd_1NiR. We also used fluorescence spectroscopy to investigate cd_1NiR dimerization and the interactions of cd_1NiR with artificial and native membranes as well as with *c*NOR. Our data implies interference from cd_1NiR binding on electron donation to *c*NOR, consistent with an overlapping interaction surface. This effect of cd_1NiR on *c*NOR activity shows a titration profile consistent with an interaction primarily with a single cd_1NiR monomer. Our fluorescence data is consistent with this dimerization occurring in the relevant concentration range (20–40 nM cd_1NiR). However, we could not observe any clear long-lived high-affinity binding between cd_1NiR and *c*NOR going beyond the rather high affinity cd_1NiR showed to artificial membranes, nor could we observe a large fraction of the cd_1NiR associated with the membrane-bound *c*NOR in *P. denitrificans* membranes. Potential *in vivo* consequences of our results are discussed.

Results

The influence of cd_1NiR on catalytic activity of *c*NOR. If *c*NOR and cd_1NiR interact with each other, they could influence each other's catalytic parameters, therefore we measured the influence of the presence of cd_1NiR on NO-reduction by *c*NOR (which is straightforward to measure). Surprisingly, we observed clear *inhibition* of *c*NOR-catalyzed NO-reduction in the presence of cd_1NiR, see Fig. 2a. NO-reduction by the *P. denitrificans* *c*NOR exhibits a sigmoidal curve, due to substrate inhibition[26,27] at NO > 10 µM. The value we report for *c*NOR activity is the maximum activity (k_{max}, note that this k_{max} is not a k_{cat} since there is substrate inhibition at higher [NO]) observed at ~5 µM NO. In the presence of cd_1NiR (Fig. 2a), two effects are observed; the maximum activity is lowered and the substrate inhibition pattern changes, see below.

We investigated the inhibitory effect as a function of cd_1NiR concentration added, the raw data is shown in Supporting Fig. 1, and a plot of the maximum rate as a function of added cd_1NiR is shown in Fig. 2b (and Supporting Fig. 2). The maximum activity of *c*NOR decreases gradually the more cd_1NiR is added and the effect reaches a maximum level of inhibition (~50%) at ~30 nM cd_1NiR (approximately equimolar to *c*NOR). Surprisingly, at higher concentrations of cd_1NiR, the inhibition is released (Fig. 2b), the possible reasons for this are discussed further below (see Fluorescence section). For the investigations of the influence of the electron donor described in the next section, we used the cd_1NiR concentration (and *c*NOR/cd_1NiR ratio) giving the maximum inhibition.

Electron donation to *c*NOR in the presence of cd_1NiR. In the co-crystal structure of the complex between the cd_1NiR and *c*NOR from *P. aeruginosa*[24], the interaction surface (see Fig. 1) could possibly overlap with interaction of the electron donor to *c*NOR. Thus, one reason for the inhibition observed with cd_1NiR could be that it interferes with electron donation, and we therefore studied the titration behavior of electron donors for *c*NOR catalysis in the absence and presence of cd_1NiR.

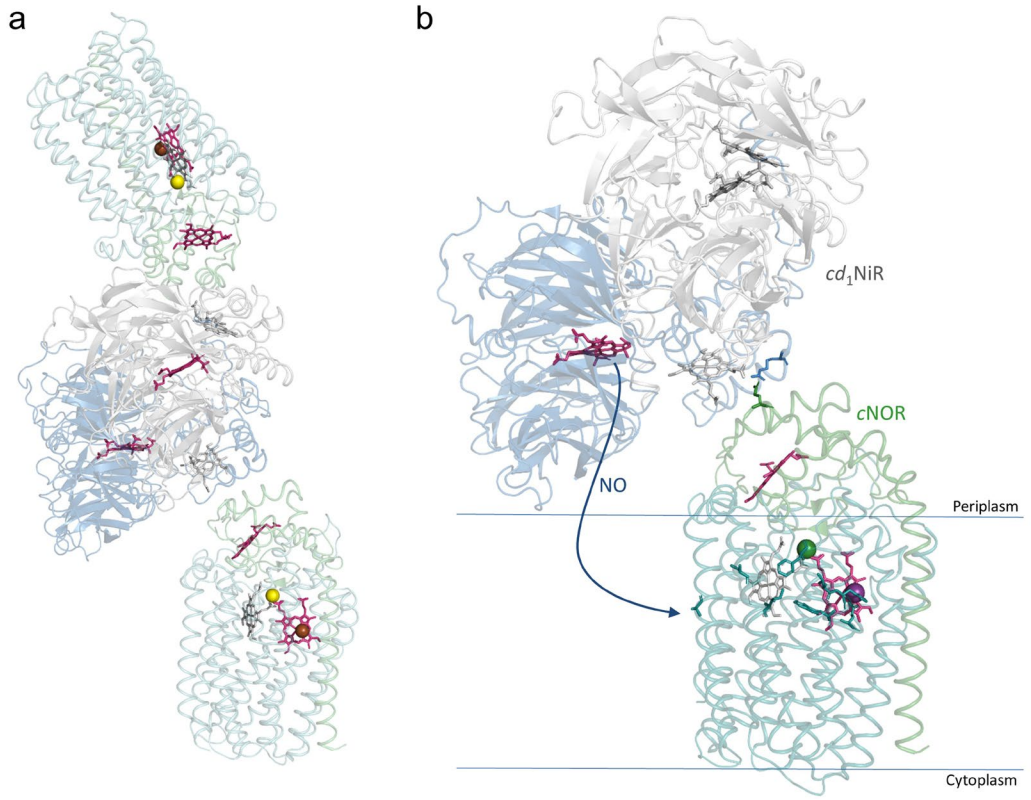

Figure 1. Structure of the co-complex of the *P. aeruginosa* *c*NOR and the cd_1NiR dimer (PDB ID: 5GUW[24]). (**a**) The full 2:2 structure with the two *c*NOR molecules in light green (NorC) and teal (NorB) and the cd_1NiR dimer in blue/gray. (**b**) Enlargement of the co-complex interaction area for cd_1NiR and a single *c*NOR, with the interaction between Arg-71 (cd_1NiR, blue stick) and Glu-119 (*c*NOR, green stick) shown. Also shown are schematic outlines of the cytoplasmic membrane in which *c*NOR sits and the path for NO from the release from the d_1 heme of cd_1NiR (pink) into the membrane from which it would travel through the suggested gas channel (indicated by green sticks) to the active site heme b_3 (pink) in *c*NOR[25]. Also highlighted is the initial electron-accepting heme *c* in NorC (pink), other heme groups in grey.

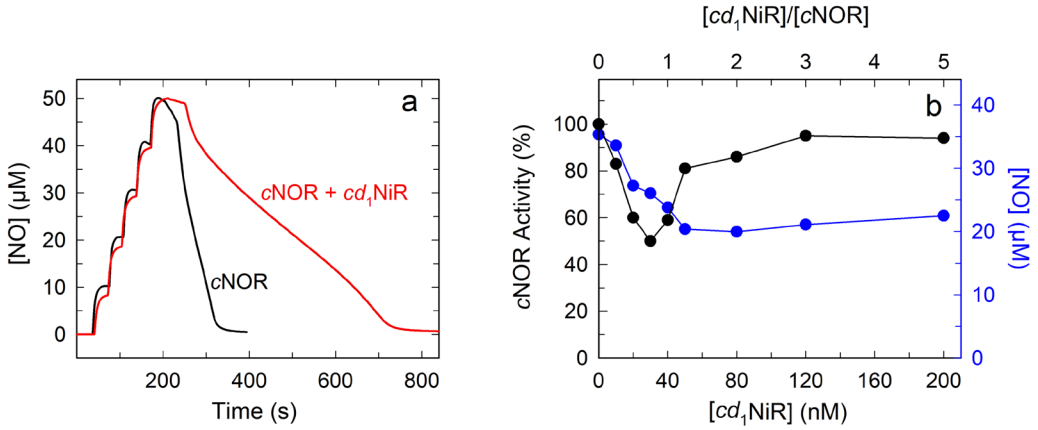

Figure 2. The inhibitory effect of cd_1NiR on *c*NOR catalysis. (**a**) NO reduction profile of *P. denitrificans* *c*NOR in the absence (black line) and presence (red line) of cd_1NiR. Experimental conditions: 50 mM HEPES pH 7.0, 50 mM KCl, 0.05% DDM, 30 mM glucose, 1 U/ml glucose oxidase, 20 U/ml catalase. Once the chamber was anaerobic, cyt. c (15 μM), TMPD (0.5 mM), and 5 times 10 μM NO (from NO-saturated water) was added. At t ~250 s, ascorbate (3 mM) and cNOR (80 nM) were added. For the trace with cd_1NiR (80 nM), it was added before the addition of NO. (**b**) Titration of the inhibitory effect of cd_1NiR on *c*NOR catalysis. Experimental conditions as in A, except the *c*NOR concentration was 40 nM, and the cd_1NiR concentration varied between 0–200 nM. *c*NOR activity (black circles) refers to the k_{max} at ~5 μM NO, with the k_{max} in the absence of cd_1NiR set at 100%. Also shown is the effect of adding cd_1NiR on substrate inhibition (blue circles) for NO-reduction by *c*NOR. The right y-axis refers to the [NO] where $k_{max}/2$ is reached (termed K_i^{app} in the text, note that this is higher than for k_{max}).

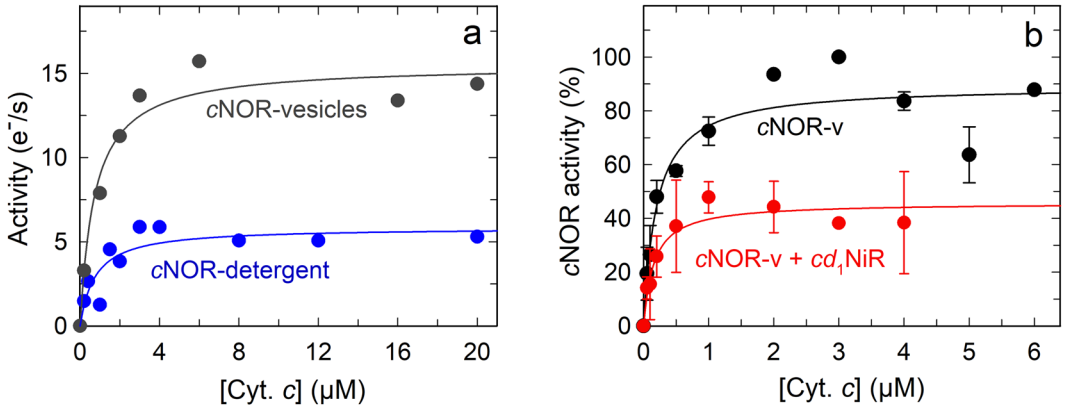

Figure 3. Determinations of the K_m for cytochrome *c* for NO reduction by *c*NOR. (**a**) Comparison between *c*NOR in detergent (blue) and reconstituted in liposomes (grey). Experimental conditions as in Fig. 2, except for with liposomes, DDM was omitted. *c*NOR activity refers to the k_{max} at ~5 μM NO with the k_{max} obtained without cyt. *c* subtracted. The lines shown are fits giving $k_{cat} = 6 \pm 1$ (e^-/(s•*c*NOR)), $K_m = 0.8 \pm 0.3$ μM cyt. *c* (blue, detergent) and $k_{cat} = 15 \pm 1$ (e^-/(s•*c*NOR)), $K_m = 0.8 \pm 0.2$ μM cyt. *c* (dark grey, liposomes). (**b**) Comparison between liposome-reconstituted *c*NOR in the absence (black) and presence (red) of cd_1NiR. *c*NOR activity refers to the k_{max} at ~5 μM NO, with the k_{max} at 3 μM cyt. *c* in the absence of cd_1NiR set at 100%. The curves were fitted as in a, giving $K_m = 0.20 \pm 0.05$ μM cyt. *c* (black, *c*NOR only) and $k_{cat} = 46 \pm 4\%$, $K_m = 0.15 \pm 0.05$ μM cyt. *c* (red, + cd_1NiR). Experimental conditions as in (**a**).

As a pre-requisite for the investigation of possible interference of electron donation caused by cd_1NiR binding to *c*NOR, we determined the K_m for cytochrome *c* (horse heart) during NO reduction by *c*NOR. For these titrations, we always used the maximum activity, k_{max} at ~5 μM NO. The results are shown in Fig. 3a and can be fitted with a $k_{max} = 6 \pm 1$ e^-s^{-1} (electrons/(s•*c*NOR)) and $K_m = 0.8 \pm 0.3$ μM. As seen in this graph, the data is scattered and the standard deviation in the K_m quite large. We therefore instead measured the activity with *c*NOR reconstituted into liposomes. The aim of this was two-fold, first the activity of *P. denitrificans* *c*NOR is higher in liposomes[17,28], giving us a larger total change in activity during titration and hence smaller relative errors. Secondly, the presence of a membrane might influence a putative *c*NOR-cd_1NiR interaction, as suggested for the *P. aeruginosa* complex[24]. In liposome-reconstituted *c*NOR, we determined the k_{max} to 15 ± 1 e^-s^{-1} and the K_m for cyt. *c* to 0.8 ± 0.2 μM (Fig. 3a), i.e. no change in K_m was observed.

Side by side experiments were conducted to determine the K_m for cyt. *c* of liposome-reconstituted *c*NOR in the absence or presence of ~30 nM cd_1NiR (Fig. 3b). This is the cd_1NiR concentration which maximally inhibits detergent-solubilized *c*NOR (Fig. 2b; see also corresponding data for liposome-reconstituted *c*NOR in Supporting Fig. 2). Surprisingly the observed K_m was unchanged in the presence of cd_1NiR ($K_m = 0.15 \pm 0.05$ μM) compared to the control ($K_m = 0.20 \pm 0.05$ μM) as shown in Fig. 3b. However, the relative k_{max} in the presence of cd_1NiR was ~50% of the control. Thus, only the k_{max} and not the K_m value is affected, indicating that the cd_1NiR and cyt. *c* do not bind at the same place to *c*NOR.

We note that the K_m value determined (in the absence of cd_1NiR) in this experiment is different from that determined in the previous experiment (Fig. 3a). This is probably due to the K_m values being low and therefore the data obtained possibly not represented well by a simple Michaelis-Menten fit. Also, the concentration of cd_1NiR is about equimolar to *c*NOR and small differences in the relative concentrations between experiments might affect the data. These considerations are the reasons for doing comparative experiments 'side-by-side'.

Since the K_m for cyt. *c* does not change significantly in the presence of cd_1NiR, we scrutinized the raw data used for Fig. 3b, and re-plotted it without subtracting the background rate (with Ascorbate (Asc)/tetramethyl-p-phenylenediamine (TMPD)) (see Supporting Fig. 3A). This shows that there is inhibition of the basal activity by cd_1NiR with only Asc/TMPD to provide electrons that does not change significantly when cyt. *c* is added. This observation suggests that cd_1NiR inhibits the electron donation from TMPD rather than that from cyt. *c*. To verify this, we studied the effect of titrating cd_1NiR on *c*NOR catalysis in the absence of TMPD (with only cyt. *c* and Asc), see Supporting Fig. 3B which shows that in the absence of TMPD, there is no inhibition.

We then studied the *c*NOR activity as a function of the TMPD concentration (with ascorbate, but in the absence of cyt. *c*), both in the absence and presence of cd_1NiR, see Fig. 4. Here there is a clear inhibition by cd_1NiR. The data indicates that there might be more than one interaction with TMPD, but assuming a single binding site, the obtained constants are; in the absence of cd_1NiR: $k_{max} = 31 \pm 2$ e^-s^{-1} and $K_m = 1.2 \pm 0.2$ mM, and in the presence of cd_1NiR: $k_{max} = 12 \pm 2$ e^-s^{-1} and $K_m = 0.7 \pm 0.2$ mM. In this scenario, both the k_{max} and K_m are affected (so-called mixed inhibition). Our data does not allow for any unambigous fit to a more complex behaviour.

We also observe inhibition by cd_1NiR when PMS is used as an electron mediator instead of TMPD (see Supporting Fig. 4). Thus, there is an inhibition of *c*NOR activity by the presence of cd_1NiR with both TMPD and PMS, indicating that the interaction surface (or part of it, cf. the data with TMPD) on *c*NOR is similar for TMPD and PMS, and that this surface overlaps with cd_1NiR binding.

As controls for the measurements described above, we studied the possibility that TMPD directly affects auto-reduction of NO, as well as the possibility that small amounts of nitrite formed (from NO) in the buffer

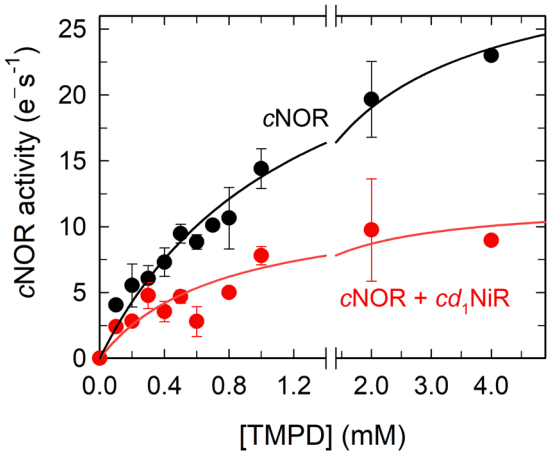

Figure 4. Determination of the K_m for TMPD for NO reduction by liposome-reconstituted *c*NOR in the absence (black) and presence (red) of cd_1NiR. Experimental conditions, and data treated as in Fig. 3. The black line is a single-hyperbolic fit to the *c*NOR data giving $k_{cat} = 31 \pm 3$ (e^-/(s•*c*NOR)), $K_m = 1.2 \pm 0.2$ mM TMPD. The red line is the same fit for the *c*NOR + cd_1NiR data, giving $k_{cat} = 10 \pm 2$ (e^-/(s•*c*NOR)), $K_m = 0.6 \pm 0.2$ mM TMPD.

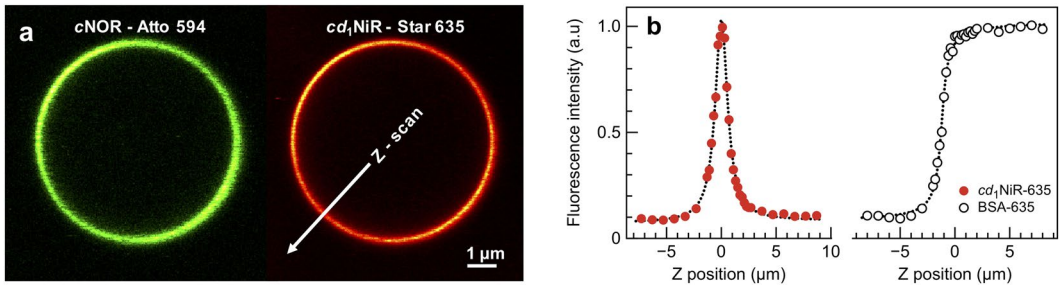

Figure 5. Fluorescently labeled *c*NOR (ATTO 594) and cd_1NiR (STAR 635) visualized with a laser scanning confocal microscope. (**a**) *c*NOR was reconstituted in giant unilamellar vesicles (GUVs) and cd_1NiR was added to the GUV solution. *c*NOR was detected in the membrane (green GUV) and cd_1NiR was found to be highly associated with the membrane (red GUV). (**b**) Fluorescence intensity scan across the membrane (Z-plane), from the inside (−) to the outside (+) of a GUV after adding cd_1NiR or BSA, labeled with STAR 635. cd_1NiR (in contrast to BSA) is highly enriched at the membrane surface. For experimental conditions, see Material and Methods.

could have effects interfering with our results. However, we found no effects that were significant enough to influence the data presented. For nitrite, we see that it can inhibit *c*NOR activity, but only at high (mM) concentrations, consistent with previous studies[29].

Substrate inhibition in *c*NOR in the presence of cd_1NiR. As described above, adding cd_1NiR during NO-reduction by *c*NOR has two effects; both reducing the maximum activity investigated above, and in changing the pattern of substrate inhibition, see Fig. 2 and Fig. S1. Thus, a plot of the NO concentration where $k_{max}/2$ is reached as a function of cd_1NiR added is shown in Fig. 2b (together with the corresponding effects on the k_{max}). Note that this refers to the NO concentration at *higher* NO (than that which gives k_{max}) where $k_{max}/2$ is reached, and therefore refers to an apparent K_i (rather than an apparent K_m). We note that the decrease in maximum rate at low cd_1NiR correlates well to the decrease in the K_i^{app} for NO (that is a higher apparent affinity for NO at an inhibitory site), whereas the K_i^{app} for NO then roughly saturates at ~40 nM cd_1NiR. It is thus clear that even though the inhibition on the maximum rate is released at higher cd_1NiR, there is still an influence also at higher cd_1NiR concentrations, indicating an interaction between *c*NOR and cd_1NiR that persists (see Discussion).

SDS page analysis for localization of cd_1NiR in *P. denitrificans*. To investigate the localization of cd_1NiR in *P. denitrificans* cells grown under denitrifying conditions, cells were fractionated, and the presence of cd_1NiR analyzed using Western blot with a specific antibody for cd_1NiR. The results, shown in Supporting Fig. 5, demonstrate that although cd_1NiR is present mainly in the periplasm, it is also found in the membrane fraction. We investigated many different conditions for this analysis including different detergents and ionic strength, but although using a milder detergent (digitonin) for solubilisation of the membrane fraction gave a somewhat larger fraction of cd_1NiR bound to it, this fraction is still small, see Discussion.

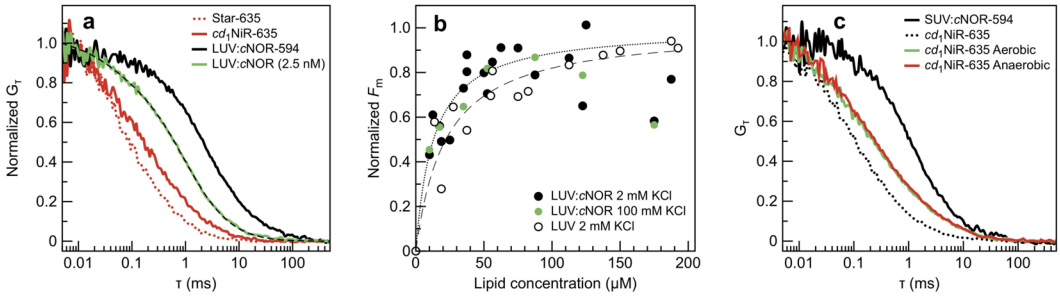

Figure 6. Interactions between cd_1NiR and liposomes, *c*NOR-liposomes and native membranes. (**a**) Fluorescence autocorrelation curves measured on a sample containing 5 nM cd_1NiR-STAR 635 (red), and after addition of LUVs containing 2.5 nM *c*NOR (green). The dashed (black) line is a fit of the data using a model with two diffusion times. As references, measurements of a sample containing free dye STAR 635 (red dotted line) and a sample with LUVs containing *c*NOR labelled with ATTO 594 are also shown. (**b**) Titration of 5 nM cd_1NiR-STAR 635 with increasing concentrations of LUVs containing unlabeled *c*NOR in buffer containing 2 mM KCl (black) or 100 mM KCl (green), and titration with the same amount of LUVs without protein (white). The plot shows the amplitude of the slow component where F_{max} has been set to 1. The data for LUVs with and without protein were fitted with a simple binding model (see text for details). (**c**) FCS curves from titration experiments with native membranes from *P. denitrificans* grown under aerobic (green) or anaerobic denitrifying (red) conditions. Sonicated membranes were added to a solution of 50 nM cd_1NiR-STAR 635 (black dotted line). A sample with DOPC-liposomes produced in the same way containing *c*NOR labelled with ATTO 594 is shown as reference (black line).

Interactions of cd_1NIR and *c*NOR investigated by fluorescence spectroscopy. Purified cd_1NiR and *c*NOR proteins were fluorescently labeled with ATTO 594 and STAR 635, respectively. *c*NOR was successfully reconstituted in giant unilamellar vesicles (GUVs), anchored to a biotin-covered glass surface imaged using a confocal laser scanning microscope (see Fig. 5a, green GUVs). cd_1NiR was then added in equimolar concentration (to *c*NOR) to the GUV solution. The cd_1NiR was also added to 'empty' GUVs. The cd_1NiR was found to be highly associated with the membrane (Fig. 5a, red GUV). A scan across the membrane (Z-plane, Fig. 5b) showed an increase in fluorescence intensity in the membrane plane (Z = 0), i.e. the concentration of cd_1NiR is higher at the membrane surface than in the surrounding solution. A control with STAR 635-labeled BSA protein (Fig. 5b) showed no such increase in the membrane plane.

The possible interaction between cd_1NiR and *c*NOR was then assayed using fluorescence correlation spectroscopy (FCS, see Methods) in combination with the confocal setup. First, we measured FCS on the reconstituted *c*NOR-ATTO 594 and cd_1NiR-STAR 635 simultaneously on the membrane surface and looked for interaction by using two-color FCS and cross-correlation analysis (FCCS). However, no significant interaction could be distinguished by this approach (Supporting Fig. 6). In agreement with this, there was no significant difference in the degree of cd_1NiR binding between the GUVs with or without *c*NOR reconstituted.

To further probe potential interactions, *c*NOR was reconstituted in DOPC liposomes (LUVs) and the interaction with cd_1NiR was assayed by monitoring changes in diffusion of labelled cd_1NiR upon binding. The diffusion time of the liposomes containing *c*NOR labelled with ATTO 594 was 2.6 ms determined with FCS (Fig. 6b, black trace). This would correspond to a liposome size of approximately 90 nm (corresponding well to the 100 nm expected from the LUV-forming protocol). Liposomes containing unlabeled *c*NOR were added in increasing concentrations to a solution containing 5 nM cd_1NiR-STAR 635. The diffusion of cd_1NiR-STAR 635 alone was 0.34 ms, corresponding to a hydrodynamic radius of ~100 Å. The addition of liposomes changed the apparent diffusion time of cd_1NiR indicating that cd_1NiR binds to the LUVs containing *c*NOR (Fig. 6). The fraction of bound cd_1NiR was determined by fitting the FCS data with a two-component diffusion model (Eq. 1), where the amplitude of the component with a long (2.6 ms) diffusion time was taken to represent liposome-bound cd_1NiR. The amplitudes of the 2.6 ms component (Fig. 6b) were fitted with a simple ligand-binding model (Eq. 2). The same experiment was repeated with 'empty' LUVs, and the binding constant for liposome binding to cd_1NiR, compared on the basis of lipid concentration, was ~13 ± 1 μM with and ~22 ± 2 μM (see Fig. 6b) without *c*NOR present in the membrane. This difference is likely within the experimental uncertainties and cd_1NiR has a similar, rather high, affinity to the liposomes independently of the presence or absence of *c*NOR.

We also increased the ionic strength in the buffer from 2 to 100 mM (KCl) in order to shield purely electrostatic interactions between cd_1NiR and the membrane. However, no decrease in the fraction bound cd_1NiR was observed (green circles in Fig. 6b) which indicates that the association of cd_1NiR to the DOPC membrane is not purely electrostatic in nature (see Discussion).

Although diffusion of both cd_1NiR and *c*NOR was detected when measuring FCS on the GUV membrane surface, there was no interaction observed using cross-correlation analysis. Thus, neither the titration experiment using small liposomes, nor the FCCS, measured directly on the membrane surface, could detect an interaction between cd_1NiR and *c*NOR going beyond the interaction between cd_1NiR and the membrane under these experimental conditions. However, it should be noted that the rather high-affinity interaction between cd_1NiR and the DOPC liposomes themselves might 'hide' a relatively weak interaction between *c*NOR and cd_1NiR, see Discussion.

Since cd_1NiR showed such significant interaction with the pure DOPC liposomes, we also wanted to investigate whether an interaction between cd_1NiR and the membrane (with or without *c*NOR expressed) could be observed using native *P. denitrificans* membranes. Small membrane vesicles were made from cells grown under either aerobic or anaerobic denitrifying conditions and mixed with a solution containing 50 nM cd_1NiR-STAR 635. Although *c*NOR expresses only during denitrifying conditions no differences were observed. The diffusion time of cd_1NiR-STAR 635 (Fig. 6c) was partly slowed down in both cases with a fraction matching the diffusion time (~1.5 ms) of sonicated DOPC liposomes containing *c*NOR-ATTO 594. In both cases the slow fraction was maximum ~ 25% of the total cd_1NiR-STAR 635 population, in comparison to up to 85% when using pure DOPC liposomes. Although these fractions do not necessarily correspond directly to the fraction bound cd_1NiR, we can conclude that cd_1NiR interacts much more strongly with artificial 'lipid-only' liposomes than it does with native membranes, see Discussion.

Dimerization of cd_1NiR. From the functional *c*NOR-catalyzed NO-reduction data presented above, the observed effect of adding increasing amounts of cd_1NiR (see Fig. 2b) made us consider that this dependence could be linked to dimerization of cd_1NiR. cd_1NiR is a dimer in the X-ray crystal structures from both *P. aeruginosa*[9,24] and *P. denitrificans*[6] and also reported to be a dimer in solution[5,30], but to our knowledge, there is no reported value for the dimerization constant. To further investigate if there is such a cd_1NiR dimer dissociation/association in the concentration range used, we analyzed the fluorescence intensity from labeled cd_1NiR as a function of its concentration. The fluorescence intensity as well as the particle number of cd_1NiR-STAR 635 obtained by FCS (parameter *N* in Eq. 1) was used to determine the photon count-rate per molecule (CPM). Figure 7 shows that the CPM increases with increasing concentrations when adding cd_1NiR-STAR 635 alone. Assuming that the majority of cd_1NiR-STAR 635 is present as a monomer at very low concentrations (<1 nM) an increase in CPM at higher concentrations indicates dimerization. In comparison, the CPM of *c*NOR labelled with the same fluorophore (*c*NOR-STAR 635) showed only a small increase, indicating that there is no change in its oligomeric state in this region.

This cd_1NiR titration was done both in the presence and absence of *c*NOR. Interestingly, both the maximum CPM for cd_1NiR-STAR 635 and its concentration dependence changed when 40 nM *c*NOR (unlabeled) was present in the solution. The CPM data could be fitted using the ligand-binding model (Eq. 2) allowing for a simple comparison; the apparent binding constants for the suggested dimerization of cd_1NiR-STAR 635 was 3.5 ± 0.1 nM without and 5.3 ± 0.2 nM with *c*NOR present. We observed a slight decrease in CPM at cd_1NiR-STAR 635 concentrations above 15 nM, but only in the case when *c*NOR was not present and these data points were not included in the fit (dashed line). The maximum CPM reached was lower in the presence of *c*NOR, indicating either a quenching effect, or that even when dimerized, the cd_1NiR is influenced by/binds *c*NOR, or that there is a fraction of cd_1NiR that cannot dimerize in the presence of *c*NOR.

Discussion

The denitrification process is tightly controlled in *P. denitrificans*, in order to avoid release and accumulation of toxic intermediates; nitric oxide and (to a lesser degree) nitrite. This control occurs on the level of transcription, by a tight coupling of the expression of the enzymes involved (see e.g.[31,32]). It has also been suggested that *in vivo*, kinetic parameters for *c*NOR are significantly different from those obtained *in vitro*, with e.g. a very high NO affinity thereby helping to keep the steady-state NO levels low[3]. A different way to minimize toxic intermediates would be to control the enzymes themselves, by e.g. forming a functional complex between cd_1NiR and *c*NOR that shuttles the NO produced from cd_1NiR directly to *c*NOR without release into the bulk phase. Support for this hypothesis was recently presented in the form of a co-complex structure of the cd_1NiR and *c*NOR from *P. aeruginosa* obtained from separately purified components[24], see Fig. 1. It should be noted that in aerobic respiration in both eukaryotes and prokaryotes, supercomplexes of individual enzyme components involved are frequently found (see e.g.[22,23,33] and references therein).

In this work, we investigated the possibility of a *c*NOR/cd_1NiR complex for *P. denitrificans*, a denitrification model bacterium. The two enzymes cd_1NiR and *c*NOR from *P. denitrificans* share 48% (*c*NOR) and 61% (cd_1NiR) overall sequence identity with their counterparts from *P. aeruginosa*. We purified the cd_1NiR from *Paracoccus pantotrophus* and not *denitrificans*, but these two enzymes are 97% identical.

The addition of cd_1NiR during NO-reduction by *c*NOR shows some intriguing effects. First, both the substrate inhibition pattern and maximum rate of NO reduction is affected by cd_1NiR (Fig. 2). Since both these parameters are presumed to be linked to the effective electron donation (see ref.[34] for a discussion on substrate inhibition), it seems plausible that a complex of cd_1NiR and *c*NOR forms and that the complex interface interferes with the access of the electron donor to *c*NOR. This conclusion is supported by the co-crystallised *Ps. aeruginosa* cd_1NiR/*c*-NOR complex[24], which shows that the cd_1NiR interacts with the NorC subunit (see Fig. 1) that harbors the initial electron acceptor (a heme *c*) of *c*NOR. As is clear from Fig. 3b (and Supporting Fig. 3) however, the observed K_m for cyt. *c* does not change in the presence of cd_1NiR but direct electron donation by TMPD is clearly affected (see Fig. 4). Although we have not used the presumed physiological c^{550} cytochrome[7,35], but the readily available horse heart (*hh*) cyt. *c*, the structures align very well and *hh* cyt. *c* works well as electron donor to *c*NOR. The small TMPD molecule (MW: 164 g/mol) presumably has a less defined or multiple interaction surfaces on *c*NOR, as indicated by our titration data (Fig. 4), and these (or some of them) presumably overlap with the interaction surface for cd_1NiR. We also observe inhibition by the presence of cd_1NiR with the electron mediator PMS (instead of TMPD, see Supporting Fig. 4).

An interesting parallel is that the antibody used for crystallisation of the *Ps. aeruginosa* *c*NOR (only)[21], was shown to interfere with electron donation from cytochrome *c*, but not from PMS[21]. The binding site for this antibody has some, albeit small, overlap with the binding of cd_1NiR in the co-crystal complex[24].

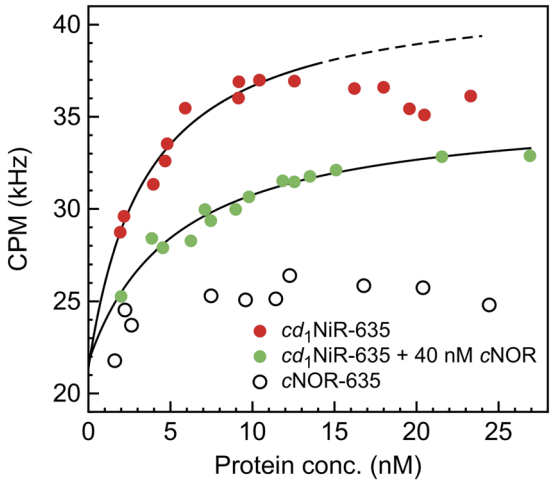

Figure 7. Fluorescence intensity (count per molecule (CPM)) when adding increasing amounts of cd_1NIR-STAR 635 to a solution with (green circles) or without (red circles) 40 nM *c*NOR. The fluorescence intensity measured with increasing concentrations of *c*NOR-STAR 635 alone is also shown (white circles). The black lines are ligand-binding fits for cd_1NiR dimerization, giving $K_D = 3.5 \pm 0.1$ nM (without) and 5.3 ± 0.2 nM (with *c*NOR) respectively.

The inhibition of *c*NOR activity observed upon addition of cd_1NiR shows a clear correlation in extent to the concentration of added cd_1NiR up until approximately equimolar amounts to *c*NOR (20–40 nM), but at higher concentrations of cd_1NiR, the inhibition is relieved. This is a surprising but highly reproducible observation which we suggest could be due to an effect of dimerization of cd_1NiR, which is purified and crystallized in the dimeric form both in *P. pantotrophus*[6] and *P. aeruginosa*[9]. Our fluorescence intensity measurements with labeled cd_1NiR showed a fluorescence 'count-rate per particle' (CPM) increase (Fig. 7), consistent with dimerization with an apparent K_D of ~3.5 nM. To our knowledge, an apparent dimerization constant for cd_1NiR has not previously been determined. In the *P. aeruginosa* cd_1NiR dimer there is domain 'swapping' between the monomers, leading to a presumably obligatory dimer, whereas no such swapping occurs in the *P. pantotrophus* (and hence *denitrificans)* cd_1NiR. This difference is likely to affect the stability of the dimer and also the propensity to interact with *c*NOR. Also consistent with our functional data is that this K_D is affected (increases) in the presence of *c*NOR, from 3.5 nM to ~5 nM, supporting an interaction between *c*NOR and cd_1NiR in the same concentration range as used in the functional assay. The total CPM for cd_1NiR is also affected by *c*NOR, and the 40 nM *c*NOR used in this experiment might not be enough to saturate the effects, such that the influence of *c*NOR for cd_1NiR dimerization might be somewhat underestimated.

The *Ps. aeruginosa* co-complex structure, where each cd_1NiR monomer binds a *c*NOR on opposite 'ends' (Fig. 1) is a structure that cannot be formed *in vivo* because of the restrictions imposed by the cytoplasmic membrane. This is thus consistent with a *c*NOR/cd_1NiR interaction that is stronger when both proteins are in their monomeric forms. In this context, we do see differences in the inhibition patterns when adding cd_1NiR to *c*NOR in detergent versus in liposomes, but qualitatively, the results are similar (see Supporting Fig. 2).

Although the effect cd_1NiR has on the maximum rate of NO-reduction was interpreted above in terms of only occurring for the monomer of cd_1NiR, even at higher cd_1NiR concentrations (i.e. when cd_1NiR is predominantly a dimer) it still influences *c*NOR catalysis as seen in the plots of the K_i^{app} (Fig. 2b). A possible interpretation for this is that cd_1NiR still interacts with *c*NOR even in its dimeric form, but that the interaction surface changes. It's also possible that the effect on the *c*NOR substrate inhibition pattern originates from structural changes occurring in cd_1NiR itself as a response to changes in [NO] or in reduction levels (as seen in[36], see below).

Even though there are clear influences on the function of *c*NOR by the presence of cd_1NiR, we could not find evidence for a high-affinity, constant complex between the *P. denitrificans* cd_1NiR and *c*NOR, as indicated e.g. by the Western Blot results (Supporting Fig. 5) and the lack of clear differences between the interactions of (fluorescently labeled) cd_1NiR with either the native aerobic or anaerobic (denitrifying) *P. denitrificans* membranes shown in Fig. 6c. Interpreting this data is complicated by the observation that there is a rather high affinity of the cd_1NiR for lipid membranes (see Figs. 5 and 6), as reported also previously[37,38]. This interaction is not purely electrostatic in nature, whereas only electrostatic interactions between the d_1 domain and the membrane were discussed for the *P. aeruginosa* cd_1NiR-*c*NOR co-complex simulations[24]. An interaction between cd_1NiR and the cytoplasmic membrane would enable the NO produced to directly dissolve into the membrane bilayer from which it can migrate to the gas channel in *c*NOR (see Fig. 1) without equilibrating with the bulk water phase even with no direct contact between the two enzymes.

Since a co-complex structure of cd_1NiR-*c*NOR exists only for the *P. aeruginosa* proteins, we overlayed the potential interaction between the two homologous proteins from *P. denitrificans*. For the *P. denitrificans* *c*NOR, we constructed a model based on the *P. aeruginosa* structure (to which it has 54% (NorB) and 47% (NorC) sequence identity), as shown in Supporting Fig. 8A, and the Glu-119 of *P. aeruginosa* *c*NOR that forms the main interaction with the *P. aeruginosa* cd_1NiR overlays well with the corresponding Asp-123 in *P. denitrificans* *c*NOR.

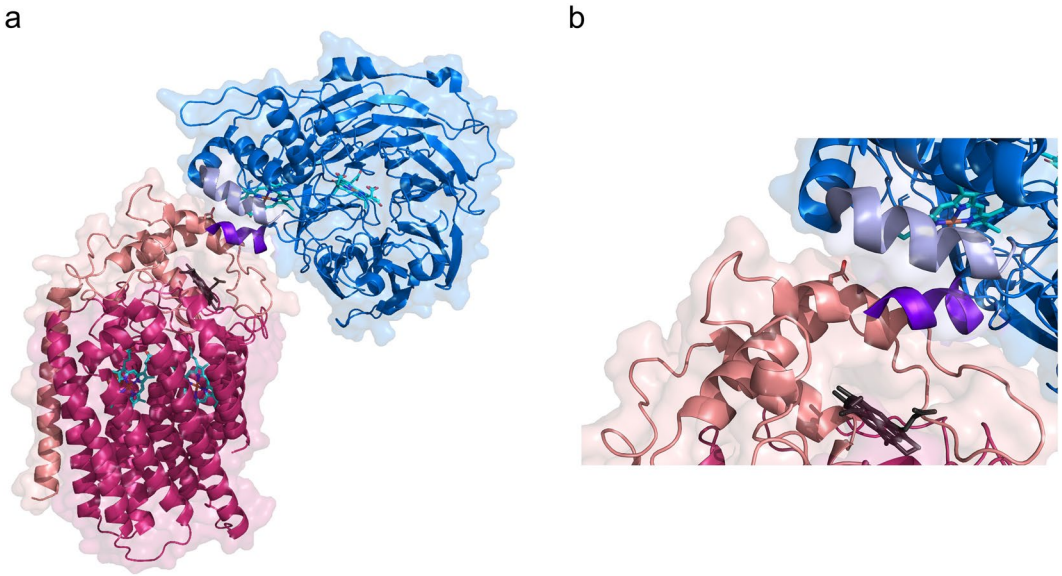

Figure 8. (**a**) The model of the *P. denitrificans* *c*NOR (NorB in magenta, NorC in salmon) and the *P. pantotrophus* cd_1NiR monomer structure (blue, PDB ID: 1QKS[6]) overlapped on the cd_1NiR/*c*NOR co-complex structure from *P. aeruginosa* (PDB ID: 5GUW[24] (not shown)). The cd_1NiR helix that interacts with NorC (in the co-complex) in light blue and the 'extra' N-terminal helix in purple. Note that this 'extra' helix would clash into the NOR/NiR interface. Shown is also the D123 (stick) of NorC (equivalent to the E-119 in *Ps. aeruginosa*) and the heme groups of the proteins. (**b**) Zoom-in of interface. The picture outlines also the surface (transparent) of the proteins except for the 'extra' helix.

However, the *P. pantotrophus* cd_1NiR structure (sequence identity 97% to *P. denitrificans* cd_1NiR) shows significant differences to the cd_1NiR from *P. aeruginosa*, and there is no Arg equivalent to the R-96 (numbering from our alignment (Supporting Fig. 7), corresponds to the R-71 in the alignment from Terasaka *et al.*[24]) that interacts with the E-119 on *c*NOR (in *P. denitrificans and P. pantotrophus* cd_1NiR, the corresponding residue is a Leu). The structural overlay of the *P. pantotrophus* and *P. aeruginosa* cd_1NiRs (see Supporting Fig. 8B) further shows that the cyt. *c* domain is more different than the d_1 domain and specifically the region on cd_1NiR that is interacting with *c*NOR in the *Ps. aeruginosa* co-crystal structure is markedly different in *P. pantotrophus* cd_1NiR, there is a small N-terminal helix that would 'clash' with the *c*NOR, as shown in Fig. 8, whereas in *Ps. aeruginosa* cd_1NiR, the N-terminal is involved in 'domain swapping' and forms part of the d_1 domain (see Supporting Fig. 8C).

However, it is also known that the *P. pantotrophus* cd_1NiR *c* domain structure is significantly different in the reduced state[36], and thus suggested to undergo large-scale conformational changes upon reduction (Supporting Fig. 9). Such changes could affect both the *c*NOR interaction and the dimerization constant, since the *c* domain of cd_1NiR 'swings' out of dimer contact in the reduced state. It is difficult to predict what would happen to a putative cd_1NiR/*c*NOR complex when cd_1NiR is reduced since the N-terminal 'clashing' helix (Fig. 8), is not even resolved in the reduced cd_1NiR structure[36], and there is hardly any overlap between the oxidised and reduced *c* domain structures (Supporting Fig. 9). Presumably the interaction between *P. denitrificans* *c*NOR and cd_1NiR, if it occurs using a similar interaction surface as in *Ps. aeruginosa*, would affect this cd_1NiR conformational change and hence could be involved in controlling cd_1NiR activity. We also note that in our functional *c*NOR assays, cd_1NiR is presumably predominantly in the reduced state (depending on if it has turned over, see[39]) since there is an excess reductant and no nitrite added.

So, are there physiological consequences of having an interaction between the cd_1NiR monomer and *c*NOR that becomes much less pronounced once the cd_1NiR dimerizes? It is possible that such regulation on the enzyme level (on top of the major transcriptional regulation) is there to fine tune flux through denitrification in response to rapidly fluctuating environmental conditions and is especially important when expression levels are low.

Materials and Methods

cd_1NiR; growth of bacteria and purification. *Paracoccus pantotrophus* (G6) was grown anaerobically and cd_1NiR purified essentially as in[5]. Briefly, bacteria were grown until OD_{600} ~0.8 in a medium containing nitrate as electron acceptor and acetate as carbon source, supplemented with 50 µg/ml kanamycin. To obtain the periplasmic fraction, the cell pellet was resuspended in 200 mL buffer containing 0.5 M sucrose, 3 mM EDTA, 100 mM Tris-HCl, pH 8.0, and 400 mg of lysozyme was added. The solution was then incubated with constant stirring at 30 °C for 40 minutes. The cell solution was then centrifuged at 25000 g for 10 min. The supernatant (containing the periplasm) was applied to a DEAE anionic-exchange column (GE Healthcare), from which bound fractions were eluted with a 0–300 mM NaCl gradient in 100 mM Tris/HCl pH 8.0. The brown-colored fractions were pooled, solid ammonium sulfate was added to 40% (w/v) and the precipitated protein removed by centrifugation at 30000 g for 30 min.

The solution was applied to a phenyl-sepharose column (GE Healthcare), and a 40-0% ammonium sulfate gradient was applied. The fractions that contained pure cd_1NiR (A^{406}/A^{280} ~1.25)[8] were pooled and concentrated. The concentration of cd_1NiR was determined by using $\varepsilon^{418} = 268\,mM^{-1}\,cm^{-1}$. For antibody generation the enzyme was further purified using size exclusion chromatography in 100 mM Tris/HCl pH 7.0 on a Superose 10/300 column (GE-Healthcare).

cNOR; growth of bacteria, protein purification and model building. Purification of *c*NOR (*P. denitrificans* overexpressed in *E. coli*) was performed as described in[18], based on the original protocol from[40]. Briefly, the plasmid pNOREX was transformed in to a JM109 strain which contained the pEC86 vector[40]. *c*NOR expression was induced by IPTG. The membranes were solubilized in 100 mM Tris, pH 7.6, 50 mM NaCl, 1 mM EDTA and 1% n-dodecyl-β-D-maltoside (DDM). The membrane solution was incubated with constant stirring for 1 hour at 4 °C. The unsolubilized membranes were removed by centrifugation, and the supernatant was applied to a Q-Sepharose high performance (GE-HealthCare) column, which was equilibrated in 20 mM Tris/HCl pH 7.6, 0.04% DDM and 5 mM NaCl. The column was washed with the same buffer but containing 250 mM NaCl and *c*NOR was eluted with a 250 mM-500 mM NaCl gradient in 20 mM Tris/HCl pH 7.6, 0.04% DDM.

The pure fractions of *c*NOR were pooled, diluted 3 times in 100 mM Tris/HCl, 50 mM NaCl, and the concentration of NaCl was lowered to below 50 mM by repeated dilution and reconcentration in concentrating vials (Millipore Merck, Ltd). Aliquots were flash frozen in liquid nitrogen and stored in −80 °C.

The structural model of *P. denitrifi*cans *c*NOR was constructed with SWISS-MODEL (https://swissmodel.expasy.org) using the default parameters and refinement procedure. The crystal structure of *Pseudomonas aeruginosa c*NOR (PDB ID: 3o0r[21], sequence identity 54% for NorB and 47% for NorC) was used as the structural template. The *P. denitrifi*cans *c*NOR could also be modelled on the *Roseobacter denitrificans c*NOR (sequence identity 75% for NorB and 69% for NorC) structure[41], but since this *c*NOR, unlike *P. denitrifi*cans *c*NOR, was found to bind a Cu^+ ion in the NorC subunit, which could potentially influence the region around the presumed interaction with cd_1NiR, we chose to use the *P. aeruginosa c*NOR–derived model.

Detection of cd_1NiR in anaerobically grown (on nitrate) *P. denitrificans* cells. *P. denitrificans* (Pd1222) cells were grown anaerobically on nitrate (32 mM) as electron acceptor at 37 °C, the cells were harvested and the periplasm was obtained by osmotic shock as described above. The pellet was sonicated, and the membranes were extracted by high-speed centrifugation (100 000 g). The different cell components (whole cell, periplasm (PL) and membrane (M) fractions) were subjected to SDS-PAGE (Invitrogen, 4–12%) analysis followed by Western blot using a PDVF membrane and an antibody against cd_1NiR, obtained from Biogenes GmbH (Germany).

Protein reconstitution in vesicles. For the generation of small unilamellar vesicles (SUVs), a solution of 40 mg/ml soybean lipids in 50 mM Tris/HCl pH 7.0, 50 mM KCl was sonicated until it became clear. 2–4 μM *c*NOR was added to the liposomes in the presence of 0.6% Na-cholate and the mixture was incubated for 1 hour at 22 °C. The detergent was then removed on a PD-10 column (GE-Healthcare). For generation of large unilamellar vesicles (LUVs), DOPC (1,2-dioleoyl-sn-glycero-3-phosphocholine) lipids dissolved in $CHCl_3$ were dried and then rehydrated to 2 mM in a 10 mM phosphate buffer (pH 7.4) with 2 mM KCl. Unilammelar liposomes were made by passing the lipid solution trough a filter with a 100 nm pore size 21 times. *c*NOR was reconstituted into the liposomes by gently solubilizing the vesicles with 0.6% Na-Cholate before adding the protein at a 10:1 molar ratio (protein: liposome), giving a protein to lipid ratio of ca. 1:3500 in the outer monolayer. The detergent was then slowly removed by dialysis at 4 °C over night.

For generation of giant unilamellar vesicles (GUVs), a 1 mM stock solution of DOPC supplemented with 1% DPPE-biotinyl (2-dioleoyl-sn-glycero-3-phosphoethanolamine-N-biotinyl) (Avanti Polar Lipids) was used according to the procedure described in[42]. *c*NOR labelled with ATTO 594 (see below) was reconstituted into the GUVs using a mild detergent treatment with DDM; the protein solution containing 1 mM DDM was mixed with 20 μl GUV-solution to a final concentration of 0.05–0.25 μM protein and 0.05 mM DDM and incubated at room temperature for 30 min. The proteo-GUVs were then diluted 20 times in a 100 mM buffered glucose solution (10 mM phosphate buffer pH 7.4, 2 mM KCl) and transferred to a LabTek microscope chamber coated with streptavidin and further incubated at room temperature for 2 h. The dilution gave a final detergent concentration of 2.5 μM DDM in the sample.

Steady-state activity measurements. The interaction between *c*NOR and cd_1NiR was investigated by studying the multiple turnover activity of *c*NOR, either in detergent (0.05% DDM) or incorporated in vesicles, using a Clark-type electrode (World Precision Instruments, WPi) as in[18]. Briefly, the activity was measured in 50 mM HEPES at pH 7.0 with 50 mM KCl at room temperature. The buffer in the reaction chamber (total volume = 1 ml) was made anaerobic by adding the glucose (30 mM)/glucose oxidase (1 U/ml)/catalase (20 U/ml) system. Substrates were added with a syringe in the following order, horse heart (*hh*) cyt. *c* (varying concentrations), TMPD at varying concentrations, 5 equal additions of 10 μM NO (from NO-saturated water), and 3 mM sodium ascorbate. *c*NOR was added at various concentrations (20–80 nM) either prior to (*c*NOR in vesicles) or after all substrate additions (detergent solubilized). cd_1NIR was added prior to the addition of NO, when specified. The data was recorded with the LabScribe2 software (WPi), and the maximum NO-reduction rate was calculated (at ~5 μM NO).

Fluorescence labelling. cd_1NiR and *c*NOR were fluorescently labelled using amino-reactive dyes. The protein concentration was set to 3 mg/ml and a 1/20 volume of $NaHCO_3$ (pH 9.0) was added. cd_1NiR was labelled with a 5-fold molar excess of Abberior STAR 635 (Abberior GmbH) and *c*NOR was labelled with a 3-fold molar excess of ATTO 594 (ATTO Tec GmbH) by incubating at room temperature while gently shaking for 1.5 h. Unbound dye was removed using a PD-10 column (GE Healthcare), equilibrated with a 10 mM phosphate buffer (pH 7.4) supplemented with 100 mM sucrose, 2 mM KCl and 1 mM (~0.05%) DDM.

Fluorescence correlation spectroscopy (FCS) measurements and analyses. FCS measurements were performed on an instrument from Abberior Instruments (Göttingen, Germany), built on a stand from Olympus (IX83), and modified for two-color imaging (see[42] for a detailed desciption of the experimental set up). Two fiber-coupled, pulsed (20 MHz) diode lasers emitting at 637 nm (PicoQuant AG, Berlin) and 594 nm (Abberior Instruments) were used for excitation, with the excitation pulses of the two lasers out of phase, to minimize cross-talk and enable fluorescence cross correlation of cd_1NiR-STAR 635 on the membrane surface of the GUVs containing *c*NOR-ATTO 595. For details on the correlation and cross correlation analysis, see[42,43].

The diffusion time of cd_1NiR-STAR 635 (5 nM) was determined with FCS in the presence of increasing concentration of LUVs, with or without reconstituted *c*NOR. Normalized autocorrelation curves of the recorded fluorescence intensity fluctuations, G(τ), were calculated using a MatLab script, and the recorded $G(\tau)$ curves were then fitted using a model for 3D-diffusion, including two diffusional components and a population of a non-fluorescent triplet state (T) with a relaxation time τ_T:

$$G(\tau) = \frac{1}{N(1-T)} \times a\left[\left[1+\frac{\tau}{\tau_{D1}}\right]^{-1}\left[1+\frac{\tau}{\beta^2\tau_{D1}}\right]^{-1/2}\right] + b\left[\left[1+\frac{\tau}{\tau_{D2}}\right]^{-1}\left[1+\frac{\tau}{\beta^2\tau_{D2}}\right]^{-1/2}\right] \times [1-T+Te^{-\frac{\tau}{\tau_T}}] \quad (1)$$

Here, τ_{D1} is the diffusion time of free cd_1NiR-STAR 635 and τ_{D2} is the diffusion time of LUV-bound cd_1NiR-STAR 635. $\beta = \omega_2/\omega_1$, where ω_2 and ω_1 denote the $1/e^2$ extension of the FCS detection volume in along and perpendicular to the excitation beam direction, respectively. N is the average number of fluorescent molecules in the detection volume, and a and b the fractions of fluorescent molecules belonging to each of the two different diffusion components (with $a+b=1$) The amplitudes of the component with diffusion time τ_{D2} were fitted with the binding model:

$$F_m = \frac{F_m^{\max} \times c_{sol}}{K_D + c_{sol}} \quad (2)$$

where F_m represents fraction of liposomes bound to cd_1NiR-STAR 635, c_{sol} represents non-bound liposomes (plotted as number of free lipids), and K_D is the binding constant defined by the concentration at which half of the liposomes are bound ($F_m = 0.5$). The value of F_m^{max} was set to unity.

Received: 19 June 2019; Accepted: 29 October 2019;
Published online: 21 November 2019

References

1. Tavares, P., Pereira, A. S., Moura, J. J. & Moura, I. Metalloenzymes of the denitrification pathway. *J. Inorg. Biochem.* **100**, 2087–2100 (2006).
2. van Spanning, R. J. M., Richardson, D. J. & Ferguson, S. J. In *Biology of the Nitrogen Cycle* 3–20 (Elsevier, 2007).
3. Hassan, J., Bergaust, L. L., Molstad, L., de Vries, S. & Bakken, L. R. Homeostatic control of nitric oxide (NO) at nanomolar concentrations in denitrifying bacteria - modelling and experimental determination of NO reductase kinetics *in vivo* in Paracoccus denitrificans. *Environ. Microbiol.* **18**, 2964–2978, https://doi.org/10.1111/1462-2920.13129 (2016).
4. Maia, L. B. & Moura, J. J. How biology handles nitrite. *Chem. Rev.* **114**, 5273–5357, https://doi.org/10.1021/cr400518y (2014).
5. Moir, J. W., Baratta, D., Richardson, D. J. & Ferguson, S. J. The purification of a cd1-type nitrite reductase from, and the absence of a copper-type nitrite reductase from, the aerobic denitrifier Thiosphaera pantotropha; the role of pseudoazurin as an electron donor. *Eur. J. Biochem.* **212**, 377–385 (1993).
6. Fulöp, V., Moir, J. W., Ferguson, S. J. & Hajdu, J. The anatomy of a bifunctional enzyme: structural basis for reduction of oxygen to water and synthesis of nitric oxide by cytochrome cd1. *Cell* **81**, 369–377 (1995).
7. Pearson, I. V., Page, M. D., van Spanning, R. J. & Ferguson, S. J. A mutant of Paracoccus denitrificans with disrupted genes coding for cytochrome c550 and pseudoazurin establishes these two proteins as the *in vivo* electron donors to cytochrome cd1 nitrite reductase. *J. Bacteriol.* **185**, 6308–6315 (2003).
8. Rinaldo, S. *et al.* Observation of fast release of NO from ferrous d(1) haem allows formulation of a unified reaction mechanism for cytochrome cd(1) nitrite reductases. *Biochem. J.* **435**, 217–225, https://doi.org/10.1042/BJ20101615 (2011).
9. Nurizzo, D. *et al.* N-terminal arm exchange is observed in the 2.15 A crystal structure of oxidized nitrite reductase from Pseudomonas aeruginosa. *Structure* **5**, 1157–1171 (1997).
10. Giuffrè, A. *et al.* The heme-copper oxidases of Thermus thermophilus catalyze the reduction of nitric oxide: evolutionary implications. *Proc. Natl. Acad. Sci. USA* **96**, 14718–14723 (1999).
11. Forte, E. *et al.* The cytochrome cbb3 from Pseudomonas stutzeri displays nitric oxide reductase activity. *Eur. J. Biochem.* **268**, 6486–6491 (2001).
12. Huang, Y., Reimann, J., Lepp, H., Drici, N. & Ädelroth, P. Vectorial proton transfer coupled to reduction of O2 and NO by a heme-copper oxidase. *Proc. Natl. Acad. Sci. USA* **105**, 20257–20262 (2008).
13. Cooper, C. E. & Brown, G. C. The inhibition of mitochondrial cytochrome oxidase by the gases carbon monoxide, nitric oxide, hydrogen cyanide and hydrogen sulfide: chemical mechanism and physiological significance. *J. Bioenerg. Biomembr.* **40**, 533–539 (2008).
14. Sarti, P., Forte, E., Mastronicola, D., Giuffre, A. & Arese, M. Cytochrome c oxidase and nitric oxide in action: molecular mechanisms and pathophysiological implications. *Biochim. Biophys. Acta* **1817**, 610–619 (2012).
15. Arjona, D., Wikström, M. & Ädelroth, P. Nitric oxide is a potent inhibitor of the cbb(3)-type heme-copper oxidases. *FEBS Lett.* **589**, 1214–1218, https://doi.org/10.1016/j.febslet.2015.03.033 (2015).
16. Culotta, E. & Koshland, D. E. Jr. NO news is good news. *Science* **258**, 1862–1865 (1992).
17. Reimann, J., Flock, U., Lepp, H., Honigmann, A. & Ädelroth, P. A pathway for protons in nitric oxide reductase from Paracoccus denitrificans. *Biochim. Biophys. Acta* **1767**, 362–373 (2007).
18. ter Beek, J., Krause, N., Reimann, J., Lachmann, P. & Ädelroth, P. The nitric-oxide reductase from Paracoccus denitrificans uses a single specific proton pathway. *J. Biol. Chem.* **288**, 30626–30635, https://doi.org/10.1074/jbc.M113.497347 (2013).
19. Bell, L. C., Richardson, D. J. & Ferguson, S. J. Identification of nitric oxide reductase activity in Rhodobacter capsulatus: the electron transport pathway can either use or bypass both cytochrome c2 and the cytochrome bc1 complex. *J. Gen. Microbiol.* **138**, 437-443 (1992).
20. Hendriks, J. H., Jasaitis, A., Saraste, M. & Verkhovsky, M. I. Proton and electron pathways in the bacterial nitric oxide reductase. *Biochemistry* **41**, 2331–2340 (2002).

21. Hino, T. *et al*. Structural basis of biological N2O generation by bacterial nitric oxide reductase. *Science* **330**, 1666–1670 (2010).
22. Schägger, H. Respiratory chain supercomplexes of mitochondria and bacteria. *Biochim. Biophys. Acta* **1555**, 154–159 (2002).
23. Lobo-Jarne, T. & Ugalde, C. Respiratory chain supercomplexes: Structures, function and biogenesis. *Semin. Cell. Dev. Biol.* **76**, 179–190, https://doi.org/10.1016/j.semcdb.2017.07.021 (2018).
24. Terasaka, E. *et al*. Dynamics of nitric oxide controlled by protein complex in bacterial system. *Proc. Natl. Acad. Sci. USA* **114**, 9888–9893, https://doi.org/10.1073/pnas.1621301114 (2017).
25. Mahinthichaichan, P., Gennis, R. B. & Tajkhorshid, E. Bacterial denitrifying nitric oxide reductases and aerobic respiratory terminal oxidases use similar delivery pathways for their molecular substrates. *Biochim. Biophys. Acta* **1859**, 712–724, https://doi.org/10.1016/j.bbabio.2018.06.002 (2018).
26. Girsch, P. & deVries, S. Purification and initial kinetic and spectroscopic characterization of NO reductase from Paracoccus denitrificans. *Biochim. Biophys. Acta* **1318**, 202–216 (1997).
27. Lachmann, P., Huang, Y., Reimann, J., Flock, U. & Ädelroth, P. Substrate control of internal electron transfer in bacterial nitric-oxide reductase. *J. Biol. Chem.* **285**, 25531–25537 (2010).
28. ter Beek, J., Kahle, M. & Ädelroth, P. Modulation of protein function in membrane mimetics: Characterization of P. denitrificans cNOR in nanodiscs or liposomes. *Biochim. Biophys. Acta* **1859**, 1951–1961, https://doi.org/10.1016/j.bbamem.2017.06.017 (2017).
29. Hendriks, J. *et al*. The active site of the bacterial nitric oxide reductase is a dinuclear iron center. *Biochemistry* **37**, 13102–13109, https://doi.org/10.1021/bi980943x (1998).
30. Pettigrew, G. W. & Moore, G. R. Cytochome cd1. *in Cytochromes c, vol. 1,, Springer-Verlag, Heidelberg*., 161–168 (1987).
31. Giannopoulos, G. *et al*. Tuning the modular Paracoccus denitrificans respirome to adapt from aerobic respiration to anaerobic denitrification. *Environ. Microbiol.* **19**, 4953–4964, https://doi.org/10.1111/1462-2920.13974 (2017).
32. Olaya-Abril, A. *et al*. Exploring the Denitrification Proteome of Paracoccus denitrificans PD1222. *Frontiers in microbiology* **9**, 1137, https://doi.org/10.3389/fmicb.2018.01137 (2018).
33. Wiseman, B. *et al*. Structure of a functional obligate complex III2IV2 respiratory supercomplex from Mycobacterium smegmatis. *Nat. Struct. Mol. Biol.* **25**, 1128–1136, https://doi.org/10.1038/s41594-018-0160-3 (2018).
34. Koutny, M. & Kucera, I. Kinetic analysis of substrate inhibition in nitric oxide reductase of Paracoccus denitrificans. *Biochem. Biophys. Res. Commun.* **262**, 562–564 (1999).
35. Thorndycroft, F. H., Butland, G., Richardson, D. J. & Watmough, N. J. A new assay for nitric oxide reductase reveals two conserved glutamate residues form the entrance to a proton-conducting channel in the bacterial enzyme. *Biochem. J.* **401**, 111–119 (2007).
36. Sjögren, T. & Hajdu, J. The Structure of an alternative form of Paracoccus pantotrophus cytochrome cd(1) nitrite reductase. *J. Biol. Chem.* **276**, 29450–29455, https://doi.org/10.1074/jbc.M103657200 (2001).
37. Mancinelli, R. L., Cronin, S. & Hochstein, L. I. The purification and properties of a cd-cytochrome nitrite reductase from Paracoccus halodenitrificans. *Arch. Microbiol.* **145**, 202–208 (1986).
38. Hole, U. H. *et al*. Characterization of the membranous denitrification enzymes nitrite reductase (cytochrome cd1) and copper-containing nitrous oxide reductase from Thiobacillus denitrificans. *Arch. Microbiol.* **165**, 55–61 (1996).
39. Richter, C. D. *et al*. Cytochrome cd1, reductive activation and kinetic analysis of a multifunctional respiratory enzyme. *J. Biol. Chem.* **277**, 3093–3100, https://doi.org/10.1074/jbc.M108944200 (2002).
40. Butland, G., Spiro, S., Watmough, N. J. & Richardson, D. J. Two conserved glutamates in the bacterial nitric oxide reductase are essential for activity but not assembly of the enzyme. *J. Bacteriol.* **183**, 189–199 (2001).
41. Crow, A., Matsuda, Y., Arata, H. & Oubrie, A. Structure of the Membrane-intrinsic Nitric Oxide Reductase from Roseobacter denitrificans. *Biochemistry* **55**, 3198–3203, https://doi.org/10.1021/acs.biochem.6b00332 (2016).
42. Sjöholm, J. *et al*. The lateral distance between a proton pump and ATP synthase determines the ATP-synthesis rate. *Sci. Rep.* **7**, 2926, https://doi.org/10.1038/s41598-017-02836-4 (2017).
43. Rigler, R., Mets, Ü., Widengren, J. & Kask, P. Fluorescence correlation spectroscopy with high count rate and low background: analysis of translational diffusion. *Eur. Biophys. J.* **22**, 169–175 (1993).

Acknowledgements

This work was supported by the Knut and Alice Wallenberg (KAW) grant 2013.0006. We are grateful to Peter Brzezinski (SU) for helpful discussions. We thank Hui (Sophie) Shu for assistance with the Western Blots.

Author contributions

Designed study: I.A., J.S., J.W., P.Ä., Performed experimental work: I.A., J.S., J.t.B. Analysed data: I.A., J.S., J.t.B., J.W., N.W., P.Ä. Wrote the manuscript: I.A., J.S., P.Ä. All authors reviewed and revised the manuscript.

Competing interests

The authors declare no competing interests.

Additional information

Supplementary information is available for this paper at https://doi.org/10.1038/s41598-019-53553-z.

Correspondence and requests for materials should be addressed to P.Ä.

Reprints and permissions information is available at www.nature.com/reprints.

Publisher's note Springer Nature remains neutral with regard to jurisdictional claims in published maps and institutional affiliations.